Unsteady Propulsion of a Two-Dimensional Flapping Thin Airfoil in a Pulsating Stream

Ernesto Sanchez-Laulhe* and Ramon Fernandez-Feria†
University of Málaga, 29071 Málaga, Spain
and
Anibal Ollero‡
University of Seville, 41092 Seville, Spain

https://doi.org/10.2514/1.J062925

The cruising velocity of animals, or robotic vehicles, that use flapping wings or fins to propel themselves is not constant but oscillates around a mean value with an amplitude usually much smaller than the mean, and a frequency that typically doubles the flapping frequency. Quantifying the effect that these velocity fluctuations may have on the propulsion of a flapping and oscillating airfoil is of great relevance to properly modeling the self-propelled performance of these animals or robotic vehicles. This is the objective of the present work, where the force and moment that an oscillating stream exerts on a two-dimensional pitching and heaving airfoil are obtained analytically using the vortical impulse theory in the linear potential flow limit. The thrust force of the flapping airfoil in a pulsating stream in this limit is obtained here for the first time. The lift force and moment derived here contain new terms in relation to the pioneering work by Greenberg (1947), which are shown quantitatively unimportant. The theoretical results obtained here are compared with existing computational data for flapping foils immersed in a stream with velocity oscillating sinusoidally about a mean value.

I. Introduction

A RENEWED interest in more precise models of the aerodynamic forces on oscillating foils, considering all the unsteady processes intervening in the fluid–foil interaction, has been motivated by the growing interest in developing biologically inspired aerial and aquatic vehicles self-propelled by flapping wings or fins [1–6]. Most aerodynamic models come from studies that consider the oscillating foil in a flow with constant freestream velocity. However, the cruising velocity of animals, or robotic vehicles, that use flapping wings or fins to propel themselves is not constant [3,7–11]. It oscillates around a mean value with an amplitude usually much smaller than the mean, and a frequency that typically doubles the flapping frequency. For instance, for a small flapping amplitude (airfoil chord length ratio, say, $\epsilon \ll 1$), the cruising velocity oscillations amplitude has been found to be of the order of $\epsilon^{2/3}$ times the mean velocity for a simple aquatic locomotion model [11], and of the order of ϵ^2 for a simple ornithopter flight model [10]. The frequency doubling is nicely illustrated by the ability of a sinusoidally plunging airfoil to produce thrust by the Knoller–Betz effect [12]. Although it has been argued that the oscillations in the flow speed have little impact on the time-averaged aerodynamic force [13], and therefore on the time-averaged cruising velocity generated by an oscillating foil, results obtained in the present work that are compared with previous numerical results show that these oscillations may modify substantially not only the instantaneous aerodynamic forces, but also their time-averaged values. Thus, the oscillations in the cruising velocity may be relevant for the unsteady dynamics of the robotic vehicle propelled by the flapping foil, and therefore for its guidance and control. The objective of the present work is to include and quantify this effect of a periodic streamwise velocity about a mean value on the time-dependent thrust force generated by a pitching and heaving foil in the limit of small flapping amplitudes and high Reynolds numbers, so that linear potential flow theory can be applied, a limit of interest for the cruising regime of vehicles self-propelled by flapping wings or fins.

The effect of a pulsating stream on the airfoil aerodynamic forces in the linear potential and two-dimensional (2D) flow limit was considered by Isaacs [14] and Greenberg [15], partially inspired by unsteady problems related to helicopter aerodynamics. Isaacs [14] analyzed the general problem of an airfoil at constant angle of attack with a variable stream velocity, deriving an explicit formula for the lift in the particular case of a pulsating stream, consisting of a constant velocity plus a sinusoidal variation of any amplitude and frequency. The work by Greenberg [15] extended that of Theodorsen [16] for the unsteady lift force and moment on a pitching and heaving foil in a uniform current by considering a pulsating stream, adding new terms to Theodorsen's lift and moment containing time derivatives of the streamwise velocity. However, Greenberg did not consider the thrust force, and, as we shall be see below, an additional frequency term was missing in Greenberg's lift and moment. Here we shall use the linearized vortical impulse theory, already used in the pioneering work by von Kármán and Sears [17], who reproduced Theodorsen's lift force and moment for a pitching and heaving foil in a uniform stream. The impulse theory was generalized for an incompressible flow by Wu [18], and recently applied to obtain the thrust force generated by a pitching and heaving foil in a uniform stream in the linear limit [19]. This vortical impulse theory is used here to obtain the two components of the force and the moment exerted by a 2D sinusoidal head-on stream on a pitching and heaving foil, recovering Greenberg's expressions for the lift and moment, but with additional terms, and obtaining a new expression for the thrust force. We also include a nonvanishing mean angle of attack in the formulation, to cover the case of a steady foil in a streamwise pulsating freestream, and also the effect of that mean angle of attack in the expressions for the lift, moment, and thrust of a flapping foil, not included in previous theoretical formulations.

The aerodynamic performance of a 2D airfoil in a streamwise sinusoidal flow has been analyzed numerically by Lian and Shyy [20,21] as a simple model to investigate the performance of stationary and flapping wings under this particular class of gusty environments. These authors found that flapping wings can alleviate the undesirable gust effect on the lift force better than an otherwise identical stationary foil for certain flapping kinematics. These numerical results are used here to compare with the theoretical results derived in the present work.

In summary, the novelty of the present work is to use the linearized vortical impulse theory to derive general analytical expressions for

Received 20 February 2023; revision received 12 May 2023; accepted for publication 18 May 2023; published online 26 June 2023.

*Graduate Student, Fluid Mechanics Group; ernesto.slaulhe@uma.es.
†Professor, Fluid Mechanics Group; ramon.fernandez@uma.es.
‡Professor, GRVC Robotics Laboratory; aollero@us.es.

the lift, thrust, and moment of a pitching and heaving thin airfoil with a fluctuating cruising velocity. The lift and moment expressions recover previous ones, but with new terms that are shown to be quantitatively of small relevance in relation to all the other additional terms relating to the freestream fluctuations. The main result is a new general analytical expression for the thrust force, which is essential to model properly the propulsive performance of animals or robotic vehicles that use flapping wings or fins to propel themselves. Another novelty of the present work not included in previous theoretical formulations is the effect of a nonvanishing mean angle of attack in the derived general expressions for the lift, thrust, and moment, thus increasing their ranges of applicability. The problem is formulated in the next section. General expressions for the lift, thrust, and moment are derived in Sec. III, and their corresponding time averages are given in Sec. IV. Comparison with published numerical results is presented in Sec. V, concluding in Sec. VI with a brief summary and scope of the results.

II. Formulation

We consider a 2D and slender rigid foil of chord length c undergoing harmonic pitching and heaving motions with circular frequency ω and advancing in a fluid of density ρ with a horizontal velocity that also oscillates harmonically, but now with a frequency ω_1, around a constant value U_s. We use nondimensional quantities scaled with the half-chord length $c/2$, the velocity U_s, and the density ρ. The nondimensional heaving and pitching motions, and the nondimensional velocity in the $-x$ direction (see Fig. 1) are written, respectively, as

$$h(t) = h_0\Re\left[e^{ikt}\right], \qquad \alpha(t) = \alpha_s + \alpha_0\Re\left[e^{i(kt+\phi)}\right],$$
$$U(t) = 1 + \sigma\Re\left[e^{i(k_1 t+\phi_1)}\right] \tag{1}$$

where $\Re$ means real part;

$$k = \frac{\omega c}{2U_s} \quad \text{and} \quad k_1 = \frac{\omega_1 c}{2U_s} \tag{2}$$

are the nondimensional, or reduced, frequencies; t is the nondimensional time, scaled with $c/(2U_s)$; h_0, α_0, and σ are the nondimensional amplitudes of the harmonic heaving, pitching, and horizontal motions, respectively; and ϕ and ϕ_1 are the phase shifts of these two last motions in relation to the foil's heave. Also added to the formulation is a constant mean angle of attack α_s.

We assume that the Reynolds number based on U_s and c is large enough and that $h_0 \ll 1$, $|\alpha_s| \ll 1$, and $\alpha_0 \ll 1$, so that the 2D linear, potential flow theory can be applied. With the last assumptions, i.e., for $|\alpha(t)| \ll 1$, the foil approximately lies in the interval of the x axis $-1 \le x \le 1$ in a reference frame moving with it along the x direction. The pivot axis is located at an arbitrary point $x = a$ (see Fig. 1). The amplitude $\sigma \equiv U_\sigma/U_s$ of the horizontal velocity oscillations will also be assumed small (see Sec. III.C below for the exact assumption on σ). In this reference frame, the nondimensional vertical displacement and velocity of the foil are

$$z_s(x,t) = h(t) - (x-a)\alpha(t), \qquad -1 \le x \le 1 \tag{3}$$

$$v_0(x,t) = -U(t)\alpha(t) + \dot{h}(t) - (x-a)\dot{\alpha}(t) \tag{4}$$

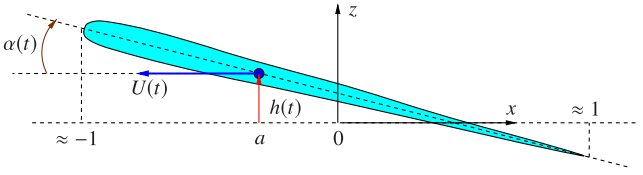

Fig. 1 Schematic of the pitching and heaving foil (nondimensional quantities).

respectively, where a dot denotes differentiation with respect to t. Note that h and v_0 are both positive upwards, while α is positive clockwise.

III. Unsteady Lift, Thrust, and Moment

The vortical impulse theory of an incompressible and unbounded flow [18,22,23] is used to obtain the forces and moment on the foil. In the linearized potential flow limit, the vorticity is concentrated at the foil interface and the trailing wake, both considered as vortex sheets along the plane $z = 0$. The expressions for the lift force and moment from this formulation were first derived by von Kármán and Sears [17], who reproduced previous results by Theodorsen [16] using a more standard linear potential flow theory, while the thrust (or minus the drag) force was derived using the vortical impulse theory in [19]. In dimensionless form they can be written as

$$C_L(t) = \frac{L(t)}{(1/2)\rho U_s^2 c} = -\frac{d}{dt}\left[\int_{-1}^{1} x\varpi_s\,\mathrm{d}x + \int_{1}^{\infty} x\varpi_e\,\mathrm{d}x\right] \tag{5}$$

$$C_T(t) = \frac{T(t)}{(1/2)\rho U_s^2 c} = -\frac{d}{dt}\left[\int_{-1}^{1} z_s\varpi_s\,\mathrm{d}x + \int_{1}^{\infty} z_e\varpi_e\,\mathrm{d}x\right] \tag{6}$$

$$C_M(t) = \frac{M(t)}{(1/2)\rho U_s^2 c^2} = \frac{1}{4}\frac{d}{dt}\left[\int_{-1}^{1} (x-a)^2\varpi_s\,\mathrm{d}x + \int_{1}^{\infty} (x-a)^2\varpi_e\,\mathrm{d}x\right] \tag{7}$$

where $L(t)$ and $T(t)$ are the forces components (per unit span) in the directions z and $-x$, respectively, and $M(t)$ is the moment (per unit span and positive when clockwise) in relation to the pitching axis $x = a$. In the last expression it must be taken into account that $da/dt = U(t)$ in a stationary reference frame with the fluid at rest far from the foil. In these expressions, $\varpi_s(x,t)$, $-1 \le x \le 1$, is the nondimensional vorticity density distribution on the foil; $\varpi_e(x,t)$ is the nondimensional vorticity density distribution in the trailing wake, both scaled with U_s; and $z_e(x,t)$ is the vertical position of each point of the vortex wake. We consider the long-time behavior in which the vortex wake sheet extends many chord lengths downstream of the airfoil, so that, in first approximation, $1 \le x \le \infty$ for both $\varpi_e(x,t)$ and $z_e(x,t)$. As aforementioned, $|z_s| \ll 1$ and $|z_e| \ll 1$.

Following von Kármán and Sears [17], the contribution from the vortex-sheet wake to $\varpi_s(x,t)$, denoted by ϖ_1, is separated from the bound circulation ϖ_0 that would produce the motion of the foil as if the wake had no effect:

$$\varpi_s(x,t) = \varpi_0(x,t) + \varpi_1(x,t), \qquad -1 \le x \le 1 \tag{8}$$

with

$$\Gamma_0(t) = \int_{-1}^{1} \varpi_0(x,t)\,\mathrm{d}x \tag{9}$$

being the nondimensional circulation (scaled with $U_s c/2$) that would be obtained from the quasi-steady foil theory, without unsteady wake. The details of the derivation of the vorticity distributions ϖ_0, ϖ_1, and ϖ_e can be found in Ref. [17] (see also Refs. [19,24]). Just a summary is given here to better appreciate the differences introduced by the unsteady stream velocity $U(t)$.

A. Vorticity Distribution

The contribution ϖ_1 from the unsteady planar wake ϖ_e, after applying Kutta's condition at the trailing edge $x = 1$, is (using the dummy variable ξ for the integration [17])

$$\varpi_1(x,t) = \frac{1}{\pi}\int_1^\infty \sqrt{\frac{\xi+1}{\xi-1}}\sqrt{\frac{1-x}{1+x}}\frac{\varpi_e(\xi,t)}{(\xi-x)}\,\mathrm{d}\xi \tag{10}$$

Kelvin's total-circulation conservation theorem requires that

$$\Gamma_0(t)+\Gamma_1(t)+\int_1^\infty \varpi_e(x,t)\,\mathrm{d}x=0,\quad \text{with}$$

$$\Gamma_1(t)=\int_{-1}^{1}\varpi_1(x,t)\,\mathrm{d}x=\int_1^\infty\left(\sqrt{\frac{\xi+1}{\xi-1}}-1\right)\varpi_e(\xi,t)\,\mathrm{d}\xi \quad (11)$$

so that it constitutes a general relation between $\Gamma_0(t)$ and $\varpi_e(x,t)$:

$$\Gamma_0(t)+\int_1^\infty\sqrt{\frac{\xi+1}{\xi-1}}\varpi_e(\xi,t)\,\mathrm{d}\xi=0 \quad (12)$$

The vorticity ϖ_0 is obtained writing the velocity field induced by the whole vorticity distribution, and imposing that the normal velocity on the foil (i.e., at $z=0$, $-1\le x\le 1$, in the present linear approximation) is the vertical velocity (4). After applying Kutta's condition at the trailing edge to fix $\Gamma_0(t)$, we obtain

$$\varpi_0(x,t)=\frac{1}{\sqrt{1-x^2}}\left[\frac{\Gamma_0}{\pi}+2(\dot h+a\dot\alpha-U\alpha)x+\dot\alpha(1\text{–}2x^2)\right] \quad (13)$$

$$\Gamma_0(t)=2\pi\left[U\alpha-\dot h-\left(a-\frac{1}{2}\right)\dot\alpha\right] \quad (14)$$

Once the vorticity distribution is known in terms of the foil motion and $\varpi_e(x,t)$, which is related to $\Gamma_0(t)$ (and therefore to the foil motion) through Eq. (12), general expressions can be obtained for Eqs. (5–7), taking into account that the wake is convected downstream with velocity $U(t)$ [17]:

$$\varpi_e(\xi,t)=\varpi_e(X),\qquad z_e(\xi,t)=z_e(X),\quad \text{with}$$
$$X=\xi-\int_{t_i}^{t}U(t)\,\mathrm{d}t \quad (15)$$

so that both ϖ_e and z_e remain constant in a reference frame where the foil moves with velocity $U(t)$; i.e., the fluid at infinity is at rest. Thus, for any function $f(\xi)$ satisfying $f(1)=0$,

$$\frac{d}{dt}\int_1^\infty f(\xi)\varpi_e(X)\,\mathrm{d}\xi=U(t)\int_1^\infty\frac{df(\xi)}{d\xi}\varpi_e(X)\,\mathrm{d}\xi \quad (16)$$

This property is valid even for the present case where U depends on time.

B. General Expressions for C_L, C_M, and C_T

Starting with the lift coefficient, after substituting the above vorticity distributions into Eq. (5), it can be written as a sum of three terms:

$$C_L(t)=C_{L0}(t)+C_{L1}(t)+C_{L2}(t) \quad (17)$$

with

$$C_{L0}(t)=-U(t)\int_1^\infty\frac{\sqrt{\xi+1}}{\sqrt{\xi-1}}\varpi_e(\xi,t)\,\mathrm{d}\xi=U(t)\Gamma_0(t) \quad (18)$$

$$C_{L1}(t)=-\frac{d}{dt}\int_{-1}^{1}x\varpi_0(x,t)\,\mathrm{d}x=\pi(\dot U\alpha+U\dot\alpha-\ddot h-a\ddot\alpha) \quad (19)$$

$$C_{L2}(t)=U(t)\int_1^\infty\frac{\varpi_e(\xi,t)}{\sqrt{\xi^2-1}}\,\mathrm{d}\xi \quad (20)$$

It is observed that, in addition to the fact that now the velocity $U(t)$ is not constant (is not unity in dimensionless form), an additional term related to its temporal derivative appears in the added mass lift (19) in relation to Theodorsen's (or von Kármán and Sears') lift coefficient. This new term was already obtained by Greenberg [15] using Theodorsen's approach instead of von Kármán and Sears' one used here. Additional terms related to the temporal variation of U will appear once the wake vorticity ϖ_e is resolved below for the harmonic motion (1). But before that it is instructive to write down the general expressions of $C_T(t)$ and $C_M(t)$ in terms of $\varpi_e(x,t)$, as just done for $C_L(t)$.

Following with $C_M(t)$, substituting Eqs. (8), (10), and (12–14) into Eq. (7), it can be written as

$$C_M(t)=C_{M0}(t)+C_{M1}(t)+C_{M2}(t)+\frac{a}{2}C_L(t) \quad (21)$$

where

$$C_{M0}(t)=\frac{1}{2}U(t)\int_{-1}^{1}x\varpi_0(x,t)\,\mathrm{d}x=\frac{1}{4}(U\Gamma_0-\pi U\dot\alpha)$$
$$=\frac{\pi}{2}U(U\alpha-\dot h-a\dot\alpha) \quad (22)$$

$$C_{M1}(t)=-\frac{1}{4}\frac{d}{dt}\int_{-1}^{1}\left(x^2-\frac{1}{2}\right)\varpi_0(x,t)\,\mathrm{d}x=\frac{\pi}{16}\ddot\alpha \quad (23)$$

$$C_{M2}(t)=-\frac{1}{4}U(t)\int_1^\infty\frac{\varpi_e(\xi,t)}{\sqrt{\xi^2-1}}\,\mathrm{d}\xi=-\frac{1}{4}C_{L2}(t) \quad (24)$$

This expression is formally the same as that derived by Theodorsen, except that now U depends on time (and, of course, the additional term proportional to $\dot U$ appearing in C_L commented on above).

The derivation of the thrust $C_T(t)$ is a bit more complex because it involves the vertical position of the wake z_e [19]. Taking into account the property (15), the position of the wake follows the successive locations of the foil's trailing edge in a reference frame where the fluid at infinity is at rest. Thus, on using Eq. (16),

$$\frac{d}{dt}\int_1^\infty z_e(x,t)\varpi_e(x,t)\,\mathrm{d}x=U(t)[h(t)-(1-a)\alpha(t)]\varpi_e(x=1,t) \quad (25)$$

where $\varpi_e(x=1,t)$ is the wake vorticity evaluated at the trailing edge ($x=1$) at any instant of time t. The other term in Eq. (6) can be written as (for simplicity we do not write explicitly the dependencies on t and/or x of the different variables)

$$\begin{aligned}\frac{d}{dt}\int_{-1}^{1}z_s\varpi_s\,\mathrm{d}x&=\frac{d}{dt}\left[(h+a\alpha)\int_{-1}^{1}\varpi_0\,\mathrm{d}x-\alpha\int_{-1}^{1}x\varpi_0\,\mathrm{d}x\right]\\&+\frac{d}{dt}\left[(h+a\alpha)\int_{-1}^{1}\varpi_1\,\mathrm{d}x-\alpha\int_{-1}^{1}x\varpi_1\,\mathrm{d}x\right]\\&=(\dot h+a\dot\alpha)\Gamma_0+(h+a\alpha)\frac{d\Gamma_0}{dt}-\dot\alpha\int_{-1}^{1}x\varpi_0\,\mathrm{d}x\\&+\alpha C_{L1}+(\dot h+a\dot\alpha)\Gamma_1+(h+a\alpha)\frac{d\Gamma_1}{dt}\\&-\dot\alpha\int_{-1}^{1}x\varpi_1\,\mathrm{d}x-\alpha\frac{d}{dt}\int_{-1}^{1}x\varpi_1\,\mathrm{d}x\end{aligned} \quad (26)$$

Taking into account that

$$\frac{d\Gamma_1}{dt}=-\frac{d\Gamma_0}{dt}-U\varpi_e(x=1,t),$$
$$\int_{-1}^{1}x\varpi_1\,\mathrm{d}x=\int_1^\infty\left(\sqrt{\xi^2-1}-\xi\right)\varpi_e\,\mathrm{d}\xi \quad (27)$$

$$\frac{d}{dt}\int_{-1}^{1}x\varpi_1\,\mathrm{d}x=U\int_1^\infty\frac{\xi}{\sqrt{\xi^2-1}}\varpi_e\,\mathrm{d}\xi-U\int_1^\infty\varpi_e\,\mathrm{d}\xi-U\varpi_e(x=1,t) \quad (28)$$

and the above expressions for Γ_0, Γ_1, and C_L, the general expression for C_T can be written as

$$C_T(t) = -\alpha(t)C_L(t) + C_{T1}(t) + C_{T2}(t) \tag{29}$$

with

$$C_{T1}(t) = \dot{\alpha}\int_{-1}^{1} x\varpi_0\,\mathrm{d}x = \pi\dot{\alpha}(\dot{h} + a\dot{\alpha} - U\alpha) \tag{30}$$

$$C_{T2}(t) = \int_1^\infty \left[\dot{h} + a\dot{\alpha} - \alpha U + \dot{\alpha}\left(\sqrt{\xi^2-1} - \xi\right)\right]\varpi_e\,\mathrm{d}\xi \tag{31}$$

This expression formally coincides with that derived in Ref. [19], but now U depends on t, with an additional term proportional to $\dot{U}$ in C_L mentioned above and with new terms in ϖ_e associated to the time dependence of $U(t)$, as discussed next for the harmonic motion (1). It is worth mentioning here that the expression for the added-mass term C_{T1} in the right-hand side of Eq. (30), derived in Ref. [19], coincides with that recently obtained by Limacher [25] for a thin airfoil, being absent in the classical thrust expression by Garrick [26].

C. Expressions of C_L, C_M, and C_T for the Harmonic Motion (1)

Substituting Eq. (1) into Eq. (14), $\Gamma_0(t)$ can be written as

$$\begin{aligned}\Gamma_0(t) = 2\pi\Re\Bigg[&\alpha_s + \left(-ikh_0 + \alpha_0 e^{i\phi} - \left(a - \frac{1}{2}\right)ik\alpha_0 e^{i\phi}\right)e^{ikt} \\ &+ \alpha_s\sigma e^{i\phi_1}e^{ik_1 t} + \frac{1}{2}\alpha_0\sigma e^{i(\phi+\phi_1)}e^{ik_2 t} + \frac{1}{2}\alpha_0\sigma e^{i(\phi-\phi_1)}e^{ik_3 t}\Bigg], \\ k_2 = k + k_1, \qquad & k_3 = k - k_1\end{aligned} \tag{32}$$

where, in addition to the frequencies k and k_1, two new frequencies k_2 and k_3 appear associated to the product term $U\alpha$. With this circulation, Kelvin's theorem (12) and the property (15) yield the wake vorticity ϖ_e. It depends on the variable

$$\begin{aligned}X &= \xi - \int_{t_i}^{t} U(t)\,\mathrm{d}t = \xi - \int_{t_i}^{t}[1 + \sigma\cos(k_1 t + \phi_1)]\,\mathrm{d}t \\ &= \xi - t - \frac{\sigma}{k_1}\sin(k_1 t + \phi_1) + \text{constant}\end{aligned} \tag{33}$$

Since σ is assumed small, following Greenberg [15] we also assume that

$$\frac{\sigma}{k_1} = \frac{2U\sigma}{\omega_1 c} \equiv k_\sigma^{-1} \ll 1 \tag{34}$$

i.e., the reduced frequency associated to the frequency and amplitude of the pulsating stream velocity, k_σ, is very large, so that the wake's phase velocity in relation to the foil is basically that of the uniform flow, $X \simeq \xi - t + \text{constant}$. Therefore, the wake vorticity can be written as the sum of five terms, corresponding to the five different dependencies with t of $\Gamma_0(t)$ in Eq. (32):

$$\begin{aligned}\varpi_e(\xi, t) = &-2\pi\alpha_s\delta(\xi - \infty) + ge^{ik(t-\xi)} + g_1 e^{ik_1(t-\xi)} \\ &+ g_2 e^{ik_2(t-\xi)} + g_3 e^{ik_3(t-\xi)}\end{aligned} \tag{35}$$

where the first term corresponds to the starting point vortex far from the foil, δ being Dirac's delta function, and the constants of the following terms are given, according to Eqs. (12) and (32), by

$$\begin{aligned}g &= -\frac{2\pi\{-ikh_0 + \alpha_0 e^{i\phi} - [a - (1/2)]ik\alpha_0 e^{i\phi}\}}{\int_1^\infty \sqrt{(\xi + 1/\xi - 1)}e^{-ik\xi}\,\mathrm{d}\xi} \\ &= \frac{4\{-ikh_0 + \alpha_0 e^{i\phi} - [a - (1/2)]ik\alpha_0 e^{i\phi}\}}{iH_0^{(2)}(k) + H_1^{(2)}(k)}\end{aligned} \tag{36}$$

$$g_1 = -\frac{2\pi\alpha_s\sigma e^{i\phi}}{\int_1^\infty \sqrt{(\xi + 1/\xi - 1)}e^{-ik_1\xi}\,\mathrm{d}\xi} = \frac{4\alpha_s\sigma e^{i\phi}}{iH_0^{(2)}(k_1) + H_1^{(2)}(k_1)} \tag{37}$$

$$g_2 = -\frac{\pi\alpha_0\sigma e^{i(\phi+\phi_1)}}{\int_1^\infty \sqrt{(\xi + 1/\xi - 1)}e^{-ik_2\xi}\,\mathrm{d}\xi} = \frac{2\alpha_0\sigma e^{i(\phi+\phi_1)}}{iH_0^{(2)}(k_2) + H_1^{(2)}(k_2)} \tag{38}$$

$$g_3 = -\frac{\pi\alpha_0\sigma e^{i(\phi-\phi_1)}}{\int_1^\infty \sqrt{(\xi + 1/\xi - 1)}e^{-ik_3\xi}\,\mathrm{d}\xi} = \frac{2\alpha_0\sigma e^{i(\phi-\phi_1)}}{iH_0^{(2)}(k_3) + H_1^{(2)}(k_3)} \tag{39}$$

One has to take the real part of these expressions, where $H_n^{(2)}(z) = J_n(z) - iY_n(z)$, $n = 0, 1$, are the Hankel functions of the second kind, related to the Bessel functions of the first and second kind J_n and Y_n, respectively [27]. It must be noticed that in the Hankel functions in g_3 we actually use $|k_3|$ instead of k_3, with $\phi - \phi_1$ when $k_3 > 0$, and $\phi_1 - \phi$ when $k_3 < 0$, in accordance with Eq. (32).

Substituting this wake vorticity into the general expressions for $C_L(t)$, $C_T(t)$, and $C_M(t)$ of the above Sec. III.B, the following expressions are obtained:

$$\begin{aligned}C_L(t) = &\pi(\dot{U}\alpha + U\dot{\alpha} - \ddot{h} - a\ddot{\alpha}) + 2\pi U\alpha_s \\ &+ U\Re[G_0\mathcal{C}(k)e^{ikt} + G_{01}\mathcal{C}(k_1)e^{ik_1 t} + G_{02}\mathcal{C}(k_2)e^{ik_2 t} \\ &+ G_{03}\mathcal{C}(k_3)e^{ik_3 t}]\end{aligned} \tag{40}$$

$$\begin{aligned}C_M(t) = &\frac{\pi}{2}\left[a\dot{U}\alpha + \left(a - \frac{1}{2}\right)U\dot{\alpha} - \left(\frac{1}{8} + a^2\right)\ddot{\alpha} - a\ddot{h}\right] + \pi\left(a + \frac{1}{2}\right)U\alpha_s \\ &+ \left(a + \frac{1}{2}\right)\frac{U}{2}\Re[G_0\mathcal{C}(k)e^{ikt} + G_{01}\mathcal{C}(k_1)e^{ik_1 t} + G_{02}\mathcal{C}(k_2)e^{ik_2 t} \\ &+ G_{03}\mathcal{C}(k_3)e^{ik_3 t}]\end{aligned} \tag{41}$$

$$\begin{aligned}C_T(t) = &-\alpha C_L + \pi\dot{\alpha}(\dot{h} + a\dot{\alpha} - U\alpha) - (\dot{h} + a\dot{\alpha} - U\alpha)2\pi\alpha_s \\ &- (\dot{h} + a\dot{\alpha} - U\alpha)\Re\left[\frac{2i}{\pi}G_0\mathcal{C}_1(k)e^{ikt} + \frac{2i}{\pi}G_{01}\mathcal{C}_1(k_1)e^{ik_1 t}\right. \\ &\left. + \frac{2i}{\pi}G_{02}\mathcal{C}_1(k_2)e^{ik_2 t} + \frac{2i}{\pi}G_{03}\mathcal{C}_1(k_3)e^{ik_3 t}\right] \\ &- \dot{\alpha}\Re\left[G_0\left(-\frac{2}{\pi k}(1 + ik)\mathcal{C}_1(k) - \frac{i}{k}\mathcal{C}(k)\right)e^{ikt}\right. \\ &+ G_{01}\left(-\frac{2}{\pi k_1}(1 + ik_1)\mathcal{C}_1 k_1 - \frac{i}{k_1}\mathcal{C}(k_1)\right)e^{ik_1 t} \\ &+ G_{02}\left(-\frac{2}{\pi k_2}(1 + ik_2)\mathcal{C}_1 k_2 - \frac{i}{k_2}\mathcal{C}(k_2)\right)e^{ik_2 t} \\ &\left. + G_{03}\left(-\frac{2}{\pi k_3}(1 + ik_3)\mathcal{C}_1 k_3 - \frac{i}{k_3}\mathcal{C}(k_3)\right)e^{ik_3 t}\right]\end{aligned} \tag{42}$$

where

$$\begin{aligned}\mathcal{C}(z) \equiv \mathcal{F}(z) + i\mathcal{G}(z) &= \frac{H_1^{(2)}(z)}{iH_0^{(2)}(z) + H_1^{(2)}(z)}, \\ \mathcal{C}_1(z) \equiv \mathcal{F}_1(z) + i\mathcal{G}_1(z) &= \frac{(1/k)e^{-iz}}{iH_0^{(2)}(z) + H_1^{(2)}(z)}\end{aligned} \tag{43}$$

with $\mathcal{C}(z)$ the well-known Theodorsen function [16,26], now applied to different reduced frequencies ($z = k, k_1, k_2$ or k_3), and

$$G_0 = 2\pi\left[-ikh_0 + \alpha_0 e^{i\phi} - ik\alpha_0 e^{i\phi}\left(a - \frac{1}{2}\right)\right] \tag{44}$$

$$G_{01} = 2\pi\sigma\alpha_s e^{i\phi_1}, \qquad G_{02} = \pi\sigma\alpha_0 e^{i(\phi+\phi_1)},$$
$$G_{03} = \pi\sigma\alpha_0 e^{i(\phi-\phi_1)} \tag{45}$$

taking into account the above comment on the signs of k_3 and $\phi - \phi_1$ in $\mathcal{C}(k_3)$ and G_{03}. Clearly, expressions (40–42) coincide with the previously known ones for a constant stream velocity [16,17,19] by setting $\sigma = 0$ (i.e., $U = 1$ and $G_{01} = G_{02} = G_{03} = 0$), except for the fact that we have also included the contributions from a nonzero mean angle of attack α_s, which appear in the above expressions just after the corresponding added-mass terms. For a steady airfoil ($h_0 = \alpha_0 = 0$) in a uniform current ($\sigma = 0$) one obviously recovers the classical expressions $C_L = 2\pi\alpha_s$, $C_M = (a + 1/2)C_L/2$, and $C_T = 0$.

The expressions for the lift and moment (40) and (41) basically coincide with those obtained by Greenberg [15] from a different approach within the linearized potential flow theory (following the work by Theodorsen [16]), except for the terms with k_3 in Eqs. (40) and (41), i.e., the terms multiplied by G_{03}, which are missing in Greenberg's expressions for the lift and moment. Probably, when considering the products of pitching and pulsating-stream terms, this author only considered the sum of frequencies, missing the frequency difference terms. However, as shown in Fig. 2 for a representative case of a pitching and heaving airfoil in a pulsating stream with $\sigma = 0.2$ that will be used below in the validation section, the differences in the results when these k_3 terms are neglected are quite small. On the other hand, Greenberg did not obtain the thrust force, derived here together with the lift and moment, though the present work has single frequency for pitching and heaving, whereas Greenberg had separate frequencies for each.

The results for a uniform freestream ($\sigma = 0$), i.e., Theodorsen's lift and moment for the same pitching and heaving motion, are also plotted in Fig. 2 (as well as in many figures in Sec. V below) to emphasize the substantial effect that the oscillating freestream may have on the aerodynamic forces and moment, not only on their instantaneous values but also on their time averages. The contributions of the new k_3 terms in C_L and C_M are negligible in comparison in all the cases we have considered. In particular, in the example plotted in Fig. 2, the maximum relative error in the instantaneous values is about 9% for C_L, with an average relative error of just 5% for C_L and slightly smaller for C_M.

Another quantity of interest is the input power, or energy transferred from the fluid to the foil per unit time and unit span, which in dimensionless form can be written as

$$C_{Pi}(t) = -C_L(t)\dot{h} - 2C_M(t)\dot{\alpha} \tag{46}$$

D. Stationary Airfoil in a Pulsating Stream

A relevant particular case of the above expressions is that of a stationary airfoil with a (small) angle of attack α_s immersed in the pulsating stream $U(t)$ defined in Eq. (1) (but now with $\phi_1 = 0$ since there is no other harmonic motion). Remember that the present linear potential flow theory is approximately valid for $|\alpha| \ll 1$, implying that the results are approximately valid for $|\alpha_s| \ll 1$, in the same sense that $2\pi\alpha_s$ is the approximate lift coefficient of a stationary airfoil in a uniform freestream for small angle of attack α_s. Setting $\alpha = \alpha_s$, $h_0 = 0$, and $\alpha_0 = 0$ in Eqs. (40–42) and rearranging some terms, the coefficients for a stationary airfoil in a pulsating stream can be written as

$$C_L(t) = \pi\dot{U}\alpha_s + 2\pi U\alpha_s(1 + \sigma\Re\{\mathcal{C}(k_1)e^{ik_1 t}\}) \tag{47}$$

$$C_M(t) = \pi a\frac{\dot{U}}{2}\alpha_s + \pi\left(a + \frac{1}{2}\right)U\alpha_s[1 + \sigma\Re\{\mathcal{C}(k_1)e^{ik_1 t}\}] \tag{48}$$

$$C_T(t) = -\pi\dot{U}\alpha_s^2 - 2\sigma U\alpha_s^2\Re\{[\pi\mathcal{C}(k_1) - 2i\mathcal{C}_1(k_1)]e^{ik_1 t}\} \tag{49}$$

This problem was also considered by Isaacs [14] from the linearized potential flow theory, but without assuming small variations of the stream velocity, i.e., without the assumption (34), and evaluating only the lift. In fact, Isaacs compared his general lift expression with the simplest, quasi-steady one where the lift is assumed proportional to the square of the unsteady stream velocity, showing with a particular example of interest in rotary wing aircraft that the results are not very different. This case, which corresponds to $k_1 = 0.0424$ and $\sigma = 0.4$, is considered in Fig. 3, comparing the present result (47) for C_L (divided by the mean

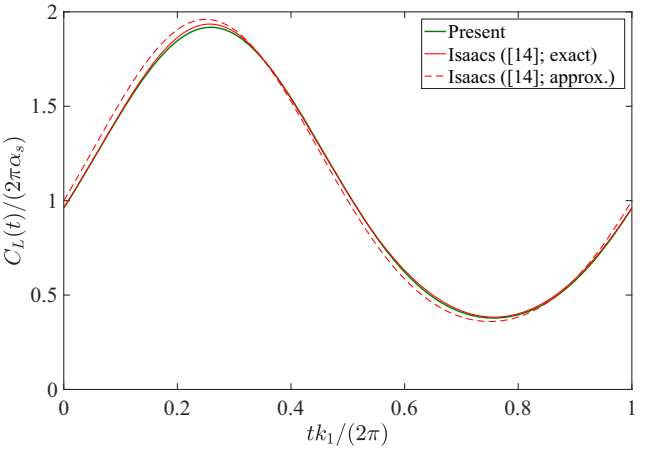

Fig. 3 $C_L(t)$ from Eq. (47) normalized with $2\pi\alpha_s$ compared with Isaac's exact and approximate (U^2) solutions [14] for $\sigma = 0.4$ and $k_1 = 0.0424$.

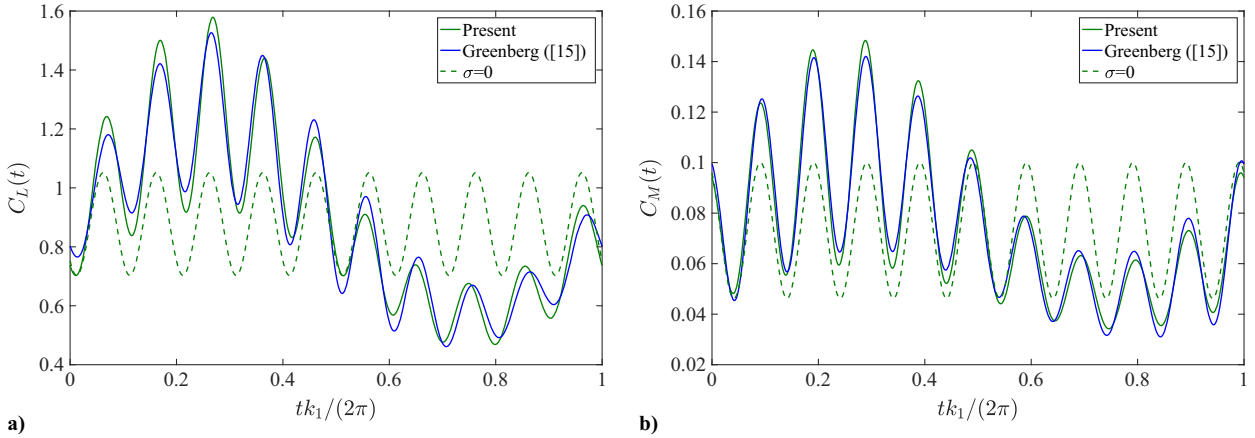

Fig. 2 $C_L(t)$ (a) and $C_M(t)$ (b) from Eqs. (40) and (41) compared with the same expressions without the k_3 terms (Greenberg): $h_0 = 0.5$, $\alpha_0 = 8.42°$, $\phi = 90°$, $k = 0.25$, $\alpha_s = 8°$, $\sigma = 0.2$, $k_1 = k/10$, and $\phi_1 = -90°$. Also plotted results for a uniform stream ($\sigma = 0$).

$2\pi\alpha_s$) with both the exact and the approximate solutions given in Isaacs's final numerical example in Ref. [14]. Note that $2\pi/k_1$ is the nondimensional period of the pulsating stream. It is observed that $C_L(t)$ from Eq. (47) is very close to Isaacs's exact solution, despite the fact that σ/k_1 is not small, significantly closer than Isaacs's approximate solution, which in the present notation is just $U^2(t)$.

IV. Time-Averaged Quantities

In many situations one is more interested in the above expressions time-averaged. Since there are different frequencies involved, one cannot average over just one of the periods. An alternative is to retain only the nonperiodic terms in the expressions, which will coincide with the time average over a cycle in pitching and heaving foils in a uniform stream. The quantities thus obtained are denoted in the expressions below with an overbar. Only the terms containing σ and/or α_s are written explicitly, using a subscript 0 to denote the corresponding values in a uniform stream with $\alpha_s = 0$ (notice that $\bar{C}_{L0} = \bar{C}_{M0} = 0$) [16,19,28].

$$\bar{C}_L = 2\pi\alpha_s\left(1 + \sigma^2\frac{\mathcal{F}(k_1)}{2}\right) \tag{50}$$

$$\bar{C}_M = \frac{1}{2}\left(a + \frac{1}{2}\right)2\pi\alpha_s\left(1 + \sigma^2\frac{\mathcal{F}(k_1)}{2}\right) \tag{51}$$

$$\bar{C}_T = \bar{C}_{T0} - (\sigma\alpha_s)^2[\pi\mathcal{F}(k_1) + 2\mathcal{G}_1(k_1)] - \frac{(\sigma\alpha_0)^2}{4}[\pi\mathcal{F}(k_2) + 2\mathcal{G}_1(k_2) + \pi\mathcal{F}(k_3) + 2\mathcal{G}_1(k_3)] \tag{52}$$

$$\bar{C}_{Pi} = \bar{C}_{Pi0} - \frac{\pi k\sigma^2 h_0\alpha_0}{4}\{\sin(\phi)[\mathcal{F}(k_2) + \mathcal{F}(k_3)] + \cos(\phi)[\mathcal{G}(k_2) + \mathcal{G}(k_3)]\} - \left(a + \frac{1}{2}\right)\frac{\pi k\sigma^2\alpha_0^2}{4}[\mathcal{G}(k_2) + \mathcal{G}(k_3)] \tag{53}$$

Another quantity of interest is the (Froude) efficiency,

$$\eta = \frac{\bar{C}_{Po}}{\bar{C}_{Pi}} \tag{54}$$

where the nondimensional, time-averaged power output coefficient is (notice that $\bar{C}_{Po0} = \bar{C}_{T0}$)

$$\begin{aligned}\bar{C}_{Po} &= U\bar{C}_T \\ &= \bar{C}_T - \pi\sigma^2\alpha_s^2\mathcal{F}(k_1) - \pi\sigma^2\alpha_0^2\left[\frac{\mathcal{F}(k)}{2} + \frac{\mathcal{F}(k_2)}{4} + \frac{\mathcal{F}(k_3)}{4} + \frac{k\mathcal{G}(k)}{2}\left(a - \frac{1}{2}\right)\right] - 2\sigma^2\alpha_s^2\mathcal{G}_1(k_1) - \sigma^2\alpha_0^2\mathcal{G}_1(k) \\ &\quad - \frac{\pi k\sigma^2 h_0\alpha_0}{2}[\mathcal{G}(k)\cos\phi - \mathcal{F}(k)\sin\phi] - \frac{k\sigma^2 h_0\alpha_0}{2}[(\mathcal{F}_1(k_2) + \mathcal{F}_1(k_3))\cos\phi - (\mathcal{G}_1(k_2) + \mathcal{G}_1(k_3))\sin\phi] \\ &\quad - \frac{ak\sigma^2\alpha_0^2}{2}[\mathcal{F}_1(k_2) + \mathcal{F}_1(k_3)] - \frac{\sigma^2\alpha_0^2}{2}[\mathcal{G}_1(k_2) + \mathcal{G}_1(k_3)] + k\sigma^2 h_0\alpha_0[\mathcal{F}_1(k)\cos\phi + \mathcal{G}_1(k)\sin\phi] \\ &\quad + k\sigma^2\alpha_0^2\mathcal{F}_1(k)\left(a - \frac{1}{2}\right) + \frac{k\sigma^2\alpha_0^2}{4}\left[2\mathcal{F}_1(k_2) + 2\mathcal{F}_1(k_3) + \frac{2\mathcal{G}_1(k_2)}{k_2} + \frac{2\mathcal{G}_1(k_3)}{k_3} + \frac{\pi\mathcal{F}(k_2)}{k_2} + \frac{\pi\mathcal{F}(k_3)}{k_3}\right]\end{aligned} \tag{55}$$

It is remarkable that the pulsating flow has no effect on the time-averaged coefficients for pure heave ($\alpha_0 = 0$) with $\alpha_s = 0$.

Some of the above time-averaged expressions are not valid when $k = k_1$, $k_1 = 2k$, and $k = 2k_1$. These special cases are summarized in the Appendix.

V. Validation

As a validation of the above theoretical results we compare them with the numerical results by Lian and Shyy [20,21]. These authors considered the effect of a sinusoidal head-on gust $U(t)$ like that in Eq. (1) (with fluctuation amplitudes $\sigma = 0.2$ and 0.5 and several values of k_1 and ϕ_1) on the aerodynamic performance of a NACA0012 airfoil at Reynolds number 4×10^4, both for a stationary airfoil with a given angle of attack α_s [20] and for plunging and pitching airfoils with several values of h_0, α_0, α_s, k, and ϕ, and the pitch axis located at quarter chord ($a = -1/2$) [21]. The numerical code and results were validated with experimental data by Anderson et al. [29] for the case of a uniform flow. The main aim of the numerical study by Lian [21] was to investigate the gust effect on the aerodynamic performance of the flapping airfoil, with the objective of finding out the best kinematics conditions to alleviate this effect and ensure a stable flight. Here, we use some of these numerical results, both for a stationary and for a flapping airfoil with the smallest pitch and heave amplitudes, to compare with the present theoretical results for C_L and C_T. No comparison to Navier–Stokes calculations of Lian and Shy corresponding to the highest amplitudes reported by these authors are shown because in these cases the leading and/or trailing edge separation, not considered in the present potential flow method, becomes very important and, consequently, the theory ceases to be valid and the agreement becomes poorer.

Figure 4 shows the comparison of the present theoretical expressions for C_L and C_T with Lian and Shyy's numerical results for a stationary NACA0012 airfoil [20], with and angle of attack $\alpha_s = 4°$ in a pulsating stream with $\sigma = 0.2$, and $k_1 = 0.085$. $U^2(t)$ is included with a dashed red line in this figure and in the following ones because it is a relevant reference for two reasons: it relates the plotted results to the velocity magnitude of the pulsating oncoming flow, and it corresponds to the quasi-static lift coefficient normalized with its time-averaged value for a given α_s. In the case of C_T, we subtract a quasi-static drag $C_{D0} = 0.05$ from the theoretical expression, as previously done in some related comparisons of potential flow theory results with numerical and experimental data [30,31]. This value is selected from the numerical results by Senturk and Smits [32] for a Reynolds number about 4×10^4. The same drag offset is used in the theoretical C_T in all the subsequent comparisons with the numerical results by Lian [21] for a flapping foil with the same Reynolds number. It is observed in Fig. 4 that the agreement between theoretical and numerical results is quite good for both $C_L(t)$ and $C_T(t)$ (the largest relative errors are about 10% for $C_L(t)$ and 15% for $C_T(t)$, and the average relative errors are approximately 5% for C_L and 7% for C_T).

Figure 5 compares the present results for $C_L(t)$ and $C_T(t)$ with numerical ones by Lian [21] for a pitching and heaving NACA0012 airfoil with $h_0 = 0.5$, $\alpha_0 = 8.42°$, $\phi = 90°$, $k = 0.25$, and $\alpha_s = 8°$, in a pulsating stream with $\sigma = 0.2$, $k_1 = k/10$, and $\phi_1 = -90°$ [notice that Lian uses $\sin(k_1 t)$ in the head-on gust instead of the $\cos(k_1 t + \phi_1)$ in Eq. (1)]. One cycle of the pulsating stream is shown, comprising 10 flapping cycles since k is 10 times k_1. There is a good agreement between the patterns of both sets of results, showing the same undulatory pattern following $U^2(t)$ (also shown in the figure). This pattern is quite different from the purely sinusoidal force histories in a uniform stream, also shown in Fig. 5 by setting $\sigma = 0$ in Eqs. (40) and (42) with the same pitching and heaving parameters. The instantaneous largest relative errors are not small [about 58% for $C_L(t)$ and 98% for $C_T(t)$], but the average relative errors over the gust cycle are much smaller (about 17% for C_L and 35% for C_T). To better appreciate this qualitative difference of the force histories for pulsating and uniform streams, Fig. 6 shows the corresponding time-averaged histories of the temporal signals plotted in Fig. 5 by computing the time averages every two flapping cycles, which are plotted in the figure as five connected symbols for each case. For a

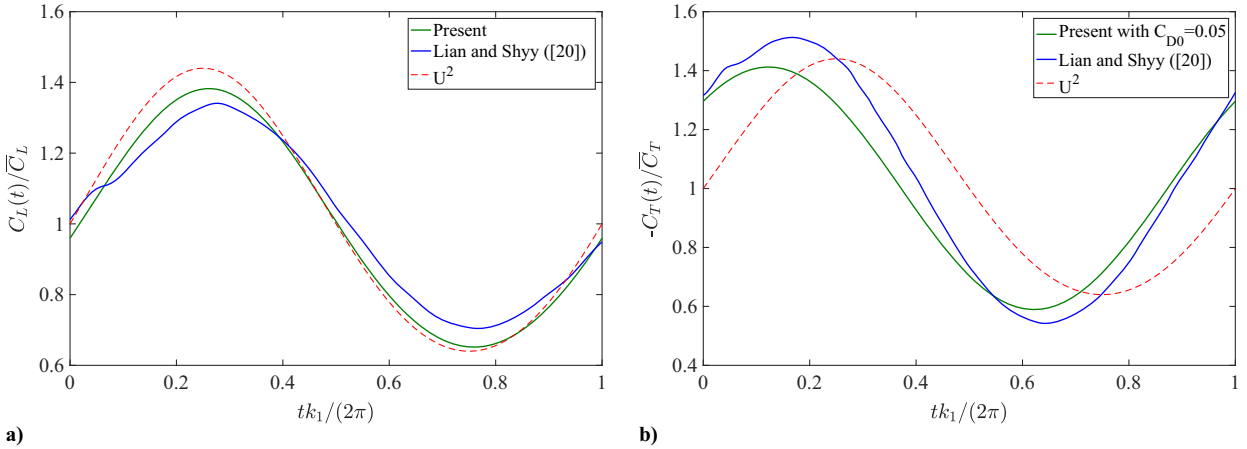

Fig. 4 Normalized $C_L(t)$ (a) and $-C_T(t)$ (b) from Eqs. (47) and (49) compared with numerical results from Fig. 20 of Lian and Shyy [20] for a stationary NACA0012 airfoil with $\alpha_s = 4°$, $\sigma = 0.2$, and $k_1 = 0.085$.

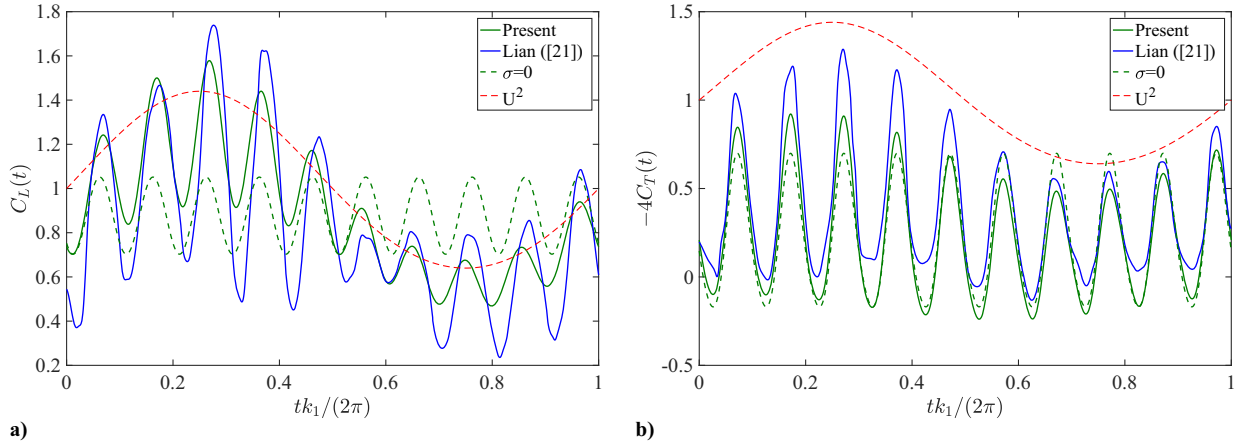

Fig. 5 $C_L(t)$ (a) and $C_T(t)$ (b) from Eqs. (40) and (42) compared with numerical results from Fig. 9 of Lian [21] for a NACA0012 airfoil with $h_0 = 0.5$, $\alpha_0 = 8.42°$, $\phi = 90°$, $k = 0.25$, and $\alpha_s = 8°$ in a stream with $\sigma = 0.2$, $k_1 = k/10$, and $\phi_1 = -90°$. Also plotted results for a uniform stream ($\sigma = 0$) and U^2 for reference sake.

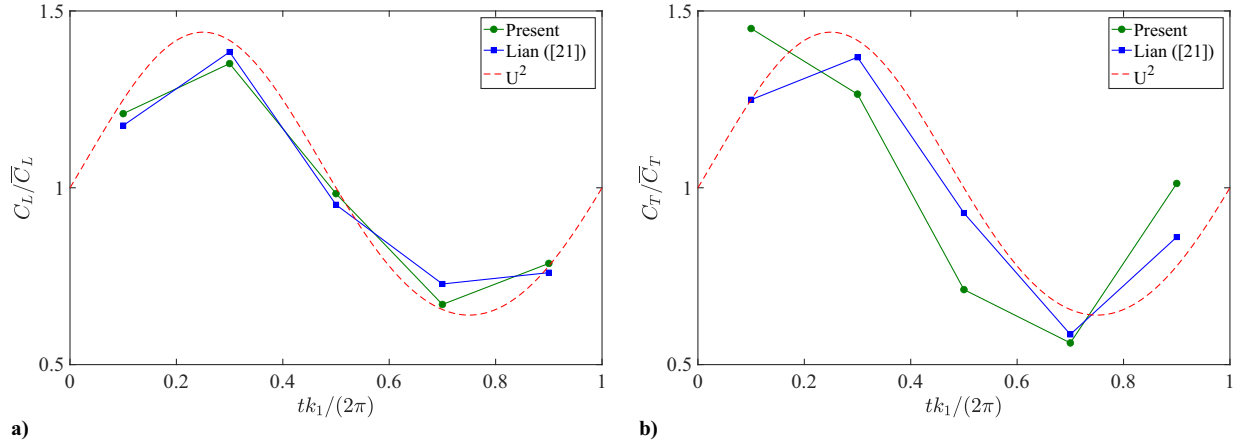

Fig. 6 Normalized time-averaged force histories corresponding to the case plotted in Fig. 5. The averages are computed every two flapping cycles, with circles corresponding to the present theoretical results and squares to Lian's numerical results (from Fig. 8 in Ref. [21]).

uniform stream (not shown), all the symbols would lie on a horizontal straight line at $y = 1$ (note that the results are normalized with the time-averaged over the complete gust cycle). The agreement is remarkable between the numerical and theoretical time-averaged lift histories [largest relative errors of about 6% for $C_L(t)$ and 22% for $C_T(t)$, and average relative errors of approximately 4% for C_L and 14% for C_T]. The agreement is apparently much better than in the instantaneous results plotted in Fig. 5, probably an effect of dividing by the overall time-averaged lift and thrust in each case. But this normalization highlights the effect of the fluctuating velocity on the aerodynamic forces, as done in the results plotted in Lian's Fig. 8 with which we compare. Also noticeable is the strong effect of a pulsating stream with an amplitude of just $\sigma = 0.2$ on both thrust and lift over a gust cycle, both following the freestream velocity pattern in this case.

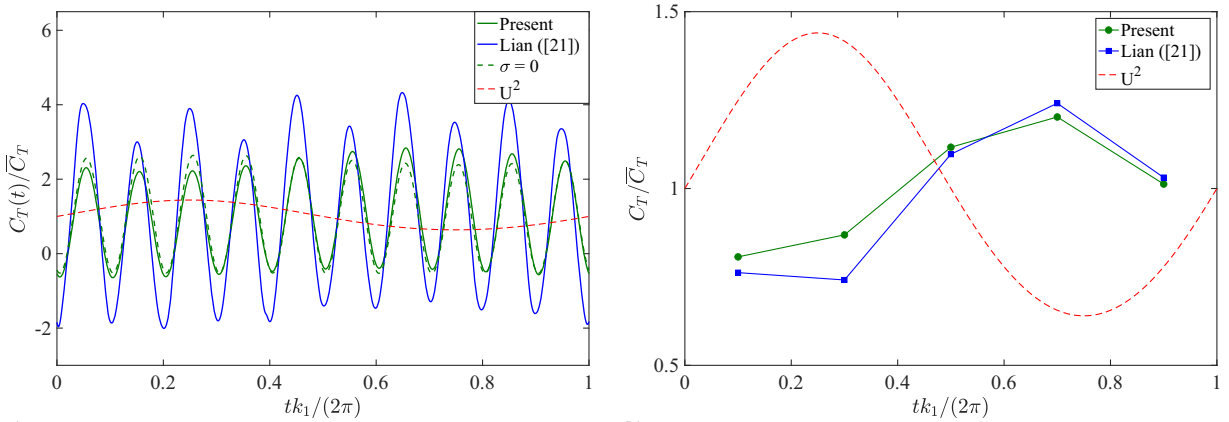

Fig. 7 Comparison between the normalized $C_T(t)$ (a) and time-averaged C_T (b) with numerical results from Fig. 11 of Lian [21] for a NACA0012 airfoil with $h_0 = 0.75, \alpha_0 = 8.42°, \phi = 75°, k = 0.63$, and $\alpha_s = 0$ in a stream with $\sigma = 0.2, k_1 = k/10$, and $\phi_1 = -90°$.

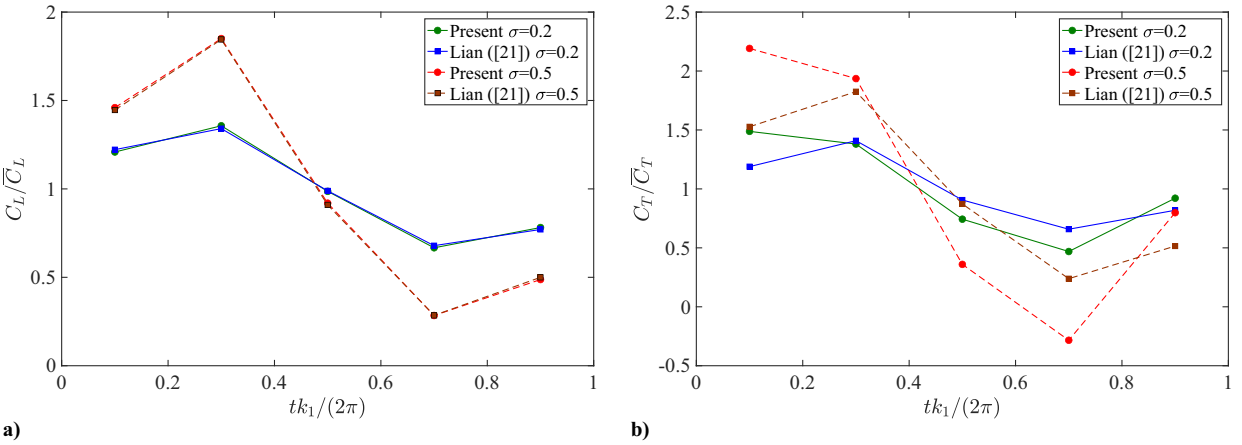

Fig. 8 Comparison between normalized time-averaged histories of C_L (a) and C_T (b) (circles) with numerical results from Fig. 8 of Lian [21] (squares) for a NACA0012 airfoil with $h_0 = 0.25, \alpha_0 = 8.42°, \phi = 90°, k = 0.25$, and $\alpha_s = 8°$ in a stream with $k_1 = k/20, \phi_1 = -90°$, and two values of σ, as indicated.

However, this is not always so, as shown in Fig. 7 for a different flapping configuration [$h_0 = 0.75, \alpha_0 = 8.42°, \phi = 75°, k = 0.63$, and $\alpha_s = 0$] in the same pulsating stream. In this case, the pattern of the time-averaged thrust history shown in Fig. 7b is opposite to that of U^2, with a smaller amplitude of the time-averaged thrust during the gust cycle than in the previous case, as it is more evident in the thrust histories shown in Fig. 7a, where the case with $\sigma = 0$ is also included. The time-averaged thrust shows less variation along the gust cycle compared to the case considered in Fig. 6, so that the gust effect of the pulsating stream seems to be alleviated with this particular flapping kinematics.

To show that the results remain accurate even for higher amplitudes and frequencies of the pulsating stream, Fig. 8 compares time-averaged lift and thrust histories for a given flapping kinematics in a pulsating stream with two amplitudes, $\sigma = 0.2$ and 0.5, and a lower frequency, $k_1 = k/20$. The time averages are now computed every four cycles, so that five points per gust cycle are shown in Fig. 8 in each case, as in previous figures with twice k_1/k. It is remarkable that there is excellent agreement between theoretical and numerical lift, which practically coincide for both values of σ (for both $\sigma = 0.2$ and $\sigma = 0.5$, the largest relative errors are about 2% and the mean relative errors about 1%), undoubtedly due to the smaller heaving amplitude in this case ($h_0 = 0.25$), thus more according with the present linear theory. Obviously, the variation along the gust cycle of the time-averaged force histories increases with the gust amplitude σ, but there are no significant differences in the comparison between theoretical and numerical results, with a much better agreement for the lift than for the thrust (the largest relative error for C_T is about 24% for $\sigma = 0.2$ and 53% for $\sigma = 0.5$, while the mean relative errors are approximately 16 and 39%, respectively). This is probably due to viscous effects that have a larger influence on the forces in the streamwise direction (due to the viscous drag) compared to the vertical (lift) direction. But in both cases, theoretical and numerical results follow the same pattern during the gust cycle. For $\sigma = 0.5$, the peaks of the time-averaged lift and thrust histories during the gust cycle are about twice their corresponding mean values (notice that the results in Fig. 8 are normalized with the corresponding mean values along the complete gust cycle).

VI. Conclusions

General expressions for the lift, thrust, and moment of a pitching and heaving airfoil immersed in a pulsating freestream are derived from linear potential flow theory using a vortical impulse formulation. The results coincide with previous ones by Greenberg [15] for the lift and moment, derived from a more standard linearized potential flow theory, except for a new circulatory term missing in Greenberg's results, which we show is quantitatively unimportant. What is more relevant is that we add here general expressions for the instantaneous and time-averaged thrust force and the corresponding propulsive efficiency.

The theoretical results are also compared with previous ones for a stationary airfoil with a given angle of attack, and validated with available numerical results by Lian and Shyy [20,21] for Reynolds number 4×10^4, several pitching and heaving kinematics and different amplitudes and frequencies of the pulsating stream, with pulsating flow frequencies 10 or more times larger than the flapping frequency. A reasonably good agreement is found with these numerical results, especially for the smallest values of the pitch and heave amplitudes considered by these authors, in accordance with the

linearized character of the present theory. The agreement is much better for the lift than for the thrust force, particularly for the time-averaged history. This is a common feature with previous linearized potential flow theories, for the viscous effects, not considered in these theories, affects the thrust more than the lift. To palliate this, a constant offset representing the viscous static drag is usually subtracted from the theoretical thrust to present a more meaningful comparison with measured or numerically computed data, as done here, but which never substitutes accurately the actual, time-varying viscous drag [9]. It is remarkable that the agreement with the numerical results remains good even for amplitudes of the pulsating stream as large as 50% of the mean freestream velocity, where peaks of the time-averaged lift and thrust over a flapping cycle may become about twice the time-averaged lift and thrust over the complete pulsating stream cycle. These strong unsteady effects in the aerodynamic forces associated to the nonstationary freestream velocity, or, equivalently, to the nonstationary cruising velocity of a self-propelled foil, may have a large impact on the propulsive performance of a flapping foil. Hence the convenience of using the expressions derived here, instead of the more conventional ones obtained for a constant stream velocity, to model the self-propulsion by a small-amplitude flapping foil.

Appendix: Time-Averaged Coefficients for Special Cases

The time-averaged coefficients for some special (integer) combinations between k and k_1 for which the general expressions in Sec. IV are not valid are summarized here. Only the coefficients that differ from those in Sec. IV are written below.

A. $k = k_1$

$$\bar{C}_L = 2\pi\left(\alpha_s + \sigma^2\frac{\mathcal{F}(k)}{2}\right) + \pi\sigma\alpha_0\cos(\phi-\phi_1) + \pi k\sigma h_0[\mathcal{G}(k)\cos(\phi_1) - \mathcal{F}(k)\sin(\phi_1)] + \pi\sigma\alpha_0[\mathcal{F}(k)\cos(\phi-\phi_1) - \mathcal{G}(k)\sin(\phi-\phi_1)] + \pi k\sigma\alpha_0[\mathcal{G}(k)\cos(\phi-\phi_1) + \mathcal{F}(k)\sin(\phi-\phi_1)]\left(a-\frac{1}{2}\right) \tag{A1}$$

$$\bar{C}_T = \bar{C}_{T0} - (\sigma\alpha_s)^2[\pi\mathcal{F}(k) + 2\mathcal{G}_1(k)] + 4k\sigma\alpha_s h_0\mathcal{G}_1(k)\sin(\phi_1) - \frac{(\sigma\alpha_0)^2}{2}\left[\frac{\pi}{2}\mathcal{F}(2k) + \mathcal{G}_1(2k)\right] - \frac{\pi k\sigma\alpha_s\alpha_0}{2}\sin(\phi_1-\phi) - \pi\sigma\alpha_s\alpha_0[\mathcal{F}(k)\cos(\phi_1-\phi) + \mathcal{G}(k)\sin(\phi_1-\phi)] - \pi k\sigma\alpha_s\alpha_0[\mathcal{G}(k)\cos(\phi_1-\phi) - \mathcal{F}(k)\sin(\phi_1-\phi)]\left(a-\frac{1}{2}\right) + 2\sigma\alpha_s\alpha_0[\mathcal{F}_1(k)\sin(\phi_1-\phi) - \mathcal{G}_1(k)\cos(\phi_1-\phi)] + k\sigma\alpha_s\alpha_0[\mathcal{F}_1(k)\cos(\phi_1-\phi) + (4a-3)\mathcal{G}_1(k)\sin(\phi_1-\phi)] \tag{A2}$$

B. $k = 2k_1$

$$\bar{C}_L = 2\pi\left(\alpha_s + \sigma^2\frac{\mathcal{F}(k)}{2}\right) + \frac{\pi\sigma^2\alpha_0}{2}[\mathcal{F}(k_1)\cos(\phi-2\phi_1) - \mathcal{G}(k_1)\sin(\phi-2\phi_1)] \tag{A3}$$

$$\bar{C}_T = \bar{C}_{T0} - (\sigma\alpha_s)^2[2\mathcal{G}_1(k_1) + \pi\mathcal{F}(k_1)] - \frac{(\sigma\alpha_0)^2}{2}\left[\frac{\pi}{2}\mathcal{F}(3k_1) + \frac{\pi}{2}\mathcal{F}(k_1) + \mathcal{G}_1(3k_1) + \mathcal{G}_1(k_1)\right] - 2\sigma^2\alpha_s\alpha_0\left[\frac{\pi}{2}\mathcal{F}(k_1) + \mathcal{G}(k_1)\right]\cos(\phi-2\phi_1) \tag{A4}$$

C. $2k = k_1$

$$\bar{C}_T = \bar{C}_{T0} - \frac{(\sigma\alpha_0)^2}{2}\left[\frac{\pi}{2}\mathcal{F}(3k_1) + \frac{\pi}{2}\mathcal{F}(k_1) + \mathcal{G}_1(3k_1) + \mathcal{G}_1(k_1)\right] - (\sigma\alpha_s)^2[2\mathcal{G}_1(k_1) + \pi\mathcal{F}(k_1)] + k\sigma h_0\alpha_0\left\{\left[2\mathcal{F}_1(k) - \frac{\pi}{2}\mathcal{G}(k)\right]\cos(\phi_1-\phi) - \left[\frac{\pi}{2}\mathcal{F}(k) + 2\mathcal{G}_1(k)\right]\sin(\phi_1-\phi)\right\} + \sigma\alpha_0^2\left\{\left[\frac{\pi k}{4} + \frac{3\pi}{2}\mathcal{G}(k) - 3\mathcal{F}_1(k) - \frac{\pi}{2}k\mathcal{F}(k)\left(a-\frac{1}{2}\right) - k\mathcal{G}_1(k)\left(2a-\frac{3}{2}\right)\right]\sin(\phi_1-2\phi) + \left[-\frac{3\pi}{2}\mathcal{F}(k) - 3\mathcal{G}_1(k) - \frac{\pi}{2}k\mathcal{G}(k)\left(a-\frac{1}{2}\right) + k\mathcal{F}_1(k)\left(2a-\frac{3}{2}\right)\right]\cos(\phi_1-2\phi)\right\} \tag{A5}$$

Acknowledgments

The authors acknowledge support from the Advanced Grant of the European Research Council GRIFFIN, Action 788247, and from the Junta de Andalucía, Spain, Grant UMA18-FEDER-JA-047. Ernesto Sanchez-Laulhe also acknowledges his predoctoral contract at the University of Malaga.

References

[1] Lauder, G. V., Anderson, E. J., Tangorra, J., and Madden, P. G. A., "Fish Biorobotics: Kinematics and Hydrodynamics of Self-Propulsion," *Journal of Experimental Biology*, Vol. 210, No. 16, 2007, pp. 2767–2780. https://doi.org/10.1242/jeb.000265

[2] Jones, K. D., and Platzer, M. F., "Design and Development Considerations for Biologically Inspired Flapping-Wing Micro Air Vehicles," *Experiments in Fluids*, Vol. 46, May 2009, pp. 799–810. https://doi.org/10.1007/s00348-009-0654-1

[3] Wen, L., Wang, T. M., Wu, G. H., and Liang, J. H., "Hydrodynamic Investigation of a Self-Propelled Robotic Fish Based on a Force-Feedback Control Method," *Bioinspiration & Biomimetics*, Vol. 7, No. 3, 2012, Paper 032012. https://doi.org/10.1088/1748-3182/7/3/036012

[4] Gerdes, J., Holness, A., Perez-Rosado, A., Roberts, L., Greisinger, A., Barnett, E., Kempny, J., Lingam, D., Yeh, C. H., Bruck, H. A., and Gupta, S. K., "Robo Raven: A Flapping-Wing Air Vehicle with Highly Compliant and Independently Controlled Wings," *Soft Robotics*, Vol. 1, No. 4, 2014, pp. 275–288. https://doi.org/10.1089/soro.2014.0019

[5] Folkertsma, G. A., Straatman, W., Nijenhuis, N., Venner, C. H., and Stramigioli, S., "Robird: A Robotic Bird of Prey," *IEEE Robotics & Automation Magazine*, Vol. 24, No. 3, 2017, pp. 22–29. https://doi.org/10.1109/MRA.2016.2636368

[6] Zhu, J., White, C., Wainwright, D. K., Di Santo, V., Lauder, G. V., and Bart-Smith, H., "Tuna Robotics: A High-Frequency Experimental Platform Exploring the Performance Space of Swimming Fishes," *Science Robotics*, Vol. 4, No. 34, 2019, Paper eaax4615. https://doi.org/10.1126/scirobotics.aax4615

[7] Alben, S., and Shelley, M., "Coherent Locomotion as an Attracting State for a Free Flapping Body," *Proceedings of the National Academy of Sciences*, Vol. 102, No. 32, 2005, pp. 11,163–11,166. https://doi.org/10.1073/pnas.0505064102

[8] Sánchez-Rodríguez, J., Raufaste, C., and Argentina, M., "A Minimal Model of Self Propelled Locomotion," *Journal of Fluids and Structures*, Vol. 97, Aug. 2020, Paper 103071. https://doi.org/10.1016/j.jfluidstructs.2020.103071

[9] Fernandez-Feria, R., Sanmiguel-Rojas, E., and Lopez-Tello, P. E., "Numerical Validation of Simple Non-Stationary Models for Self-Propelled Pitching Foils," *Ocean Engineering*, Vol. 260, Sept. 2022,

Paper 111973.
https://doi.org/10.1016/j.oceaneng.2022.111973
[10] Sanchez-Laulhe, E., Fernandez-Feria, R., and Ollero, A., "Simplified Model for Forward-Flight Transitions of a Bio-Inspired UAV," *Aerospace*, Vol. 9, No. 10, 2022, p. 617.
https://doi.org/10.3390/aerospace9100617
[11] Lopez-Tello, P. E., Fernandez-Feria, R., and Sanmiguel-Rojas, E., "Efficient Self-Propelled Locomotion by an Elastically Supported Rigid Foil Actuated by a Torque," *Applied Mathematical Modelling*, Vol. 116, April 2023, pp. 236–253.
https://doi.org/10.1016/j.apm.2022.11.007
[12] Jones, K. D., Dohring, C. M., and Platzer, M. F., "Experimental and Computational Investigation of the Knoller-Betz Effect," *AIAA Journal*, Vol. 36, No. 7, 1998, pp. 1240–1246.
https://doi.org/10.2514/2.505
[13] Van Buren, T., Floryan, D., Wei, N., and Smits, A. J., "Flow Speed Has Little Impact on Propulsive Characteristics of Oscillating Foils," *Physical Review Fluids*, Vol. 3, No. 1, 2018, Paper 013103.
https://doi.org/10.1103/PhysRevFluids.3.013103
[14] Isaacs, R., "Airfoil Theory for Flows of Variable Velocity," *Journal of the Aeronautical Sciences*, Vol. 12, No. 1, 1945, pp. 113–117.
https://doi.org/10.2514/8.11202
[15] Greenberg, J. M., "Airfoil in Sinusoidal Motion in a Pulsating Stream," NACA TR-1326, 1947.
[16] Theodorsen, T., "General Theory of Aerodynamic Instability and the Mechanism of Flutter," NACA TR-496, 1935.
[17] von Kármán, T., and Sears, W. R., "Airfoil Theory for Non-Uniform Motion," *Journal of the Aeronautical Sciences*, Vol. 5, No. 10, 1938, pp. 379–390.
https://doi.org/10.2514/8.674
[18] Wu, J. C., "Theory for the Aerodynamic Force and Moment in Viscous Flows," *AIAA Journal*, Vol. 19, No. 4, 1981, pp. 432–441.
https://doi.org/10.2514/3.50966
[19] Fernandez-Feria, R., "Linearized Propulsion Theory of Flapping Airfoils Revisited," *Physical Review Fluids*, Vol. 1, No. 8, 2016, Paper 084502.
https://doi.org/10.1103/PhysRevFluids.1.084502
[20] Lian, Y., and Shyy, W., "Aerodynamics of Low Reynolds Number Plunging Airfoil Under Gusty Environment," *45th AIAA Aerospace Sciences Meeting and Exhibit*, AIAA Paper 2007-0071, 2007.
[21] Lian, Y., "Numerical Study of a Flapping Airfoil in Gusty Environments," *27th AIAA Applied Aerodynamics Conference*, AIAA Paper 2009-3952, 2009.
[22] Saffman, P., *Vortex Dynamics*, Cambridge Univ. Press, New York, 1992, Chap. 3.
[23] Wu, J.-Z., Ma, H.-Y., and Zhou, M.-D., *Vorticity and Vortex Dynamics*, Springer, Berlin, 2006, Chap. 11.
[24] Fernandez-Feria, R., and Alaminos-Quesada, J., "Unsteady Thrust, Lift and Moment of a Two-Dimensional Flapping Thin Airfoil in the Presence of Leading-Edge Vortices: A First Approximation from Linear Potential Theory," *Journal of Fluid Mechanics*, Vol. 851, Sept. 2018, pp. 344–373.
https://doi.org/10.1017/jfm.2018.505
[25] Limacher, E. J., "Added-Mass Force on Elliptic Airfoils," *Journal of Fluid Mechanics*, Vol. 926, Nov. 2021, p. R2.
https://doi.org/10.1017/jfm.2021.741
[26] Garrick, I. E., "Propulsion of a Flapping and Oscillating Airfoil," NACA TR-567, 1936.
[27] Olver, F. W. J., and Maximon, L. C., "Bessel Functions," *NIST Handbook of Mathematical Functions*, edited by F. W. J. Olver, D. W. Lozier, R. F. Boisvert, and C. W. Clark, Cambridge Univ. Press, Cambridge, England, U.K., 2010, pp. 215–286.
[28] Alaminos-Quesada, J., and Fernandez-Feria, R., "Propulsion of a Foil Undergoing a Flapping Undulatory Motion from the Impulse Theory in the Linear Potential Limit," *Journal of Fluid Mechanics*, Vol. 883, Jan. 2020, p. A19.
https://doi.org/10.1017/jfm.2019.870
[29] Anderson, J. M., Streitlien, K., Barret, K. S., and Triantafyllou, M. S., "Oscillating Foils of High Propulsive Efficiency," *Journal of Fluid Mechanics*, Vol. 360, April 1998, pp. 41–72.
https://doi.org/10.1017/S0022112097008392
[30] Mackowski, A. W., and Williamson, C. H. K., "Direct Measurement of Thrust and Efficiency of an Airfoil Undergoing Pure Pitching," *Journal of Fluid Mechanics*, Vol. 765, Feb. 2015, pp. 524–543.
https://doi.org/10.1017/jfm.2014.748
[31] Fernandez-Feria, R., "Note on Optimum Propulsion of Heaving and Pitching Airfoils from Linear Potential Theory," *Journal of Fluid Mechanics*, Vol. 826, Sept. 2017, pp. 781–796.
https://doi.org/10.1017/jfm.2017.500
[32] Senturk, U., and Smits, A. J., "Reynolds Number Scaling of the Propulsive Performance of a Pitching Airfoil," *AIAA Journal*, Vol. 57, No. 7, 2019, pp. 2663–2669.
https://doi.org/10.2514/1.J058371

D. Zhao
Associate Editor